

Elastic Scattering of Identical Spin-Zero Nuclei

D. A. BROMLEY,* J. A. KUEHNER, AND E. ALMQVIST

Atomic Energy of Canada Limited, Chalk River Laboratories, Chalk River, Ontario, Canada

(Received March 27, 1961)

Elastic scattering measurements have been carried out on the $C^{12}+C^{12}$ and $O^{16}+O^{16}$ systems in the energy range from 6 to 35 Mev using heavy-ion beams from the Chalk River tandem accelerator and Au-Si surface barrier detectors. At energies below the Coulomb barriers the Mott scattering predictions are in excellent accord with the measurements as functions of both angle and energy. At energies above the barrier the O+O excitation curve drops exponentially below the Mott predictions to a value of 10 mb/sr at $E_{c.m.} = 16.5$ Mev and remains approximately constant thereafter at that value; in contrast, the C+C excitation curve shows marked resonant interference structure. The states involved have $\tau \gtrsim 10^{-21}$ sec, large compound elastic branching ratios Γ_e/Γ , and appear to correspond to resonant absorption of high-order partial waves, hence have high angular momentum. It is suggested that these states reflect a quasi-molecular interaction mechanism which is involved in grazing collisions of these nuclei and which is critically dependent upon the structure of the nuclei involved.

INTRODUCTION

EXTENSIVE measurements on the elastic scattering of N^{14} ions on a variety of target nuclei have been carried out with the 63-in. Oak Ridge cyclotron.¹ More recently, measurements have been reported on the elastic scattering of C^{12} and O^{16} ions from several targets using the heavy-ion linear accelerators at Yale² and Berkeley,³ respectively. The reader is referred to the *Proceedings of the First and Second Conferences on Reactions Between Complex Nuclei* for detailed references to much of this work.⁴

With the availability of heavy-ion beams of more precisely controlled and variable energy from the Chalk River tandem accelerator and of Au-Si surface barrier and diffused Si p - n junction detectors⁵ inherently well suited to heavy-ion measurements, a program of study

of heavy-ion elastic scattering⁶ and reactions⁷ has been initiated. This paper is the first in a series planned to present the data thus obtained and will describe elastic scattering measurements with C^{12} ions on carbon targets and with O^{16} ions on SiO targets.

The carbon+carbon and oxygen+oxygen systems were selected for initial study not only because of the intrinsic interest in examining the scattering of identical spin-zero bosons but also because it was hoped that any significant differences in the results obtained might be interpretable in terms of the specific nuclear structures of the ions involved. Furthermore, a detailed knowledge of the scattering from carbon and oxygen is essential in the interpretation of further scattering experiments when effects arising from carbon and oxygen target contaminants must be identified.

The pure Coulomb scattering of identical particles was first considered by Mott.⁸ The differential cross section in the center-of-mass system for scattering of identical particles of charge Ze is given by

$$d\sigma/d\Omega = (Z^4 e^4 / 16E^2) \left| \csc^2(\phi/2) \exp[-i\eta \ln \sin^2(\phi/2)] \pm \sec^2(\phi/2) \exp[-i\eta \ln \cos^2(\phi/2)] \right|^2, \quad (1)$$

where ϕ is the center-of-mass scattering angle, E is the center-of-mass energy and where the \pm signs are appropriate to systems with symmetric and antisymmetric space wave functions, respectively, and thus to the statistics of the particles involved. If the particles have intrinsic spin I , it can readily be shown⁹ that of the $(2I+1)^2$ possible independent spin wave functions for the pair, $(I+1)(2I+1)$ are symmetric, whereas

* Present address: Department of Physics, Yale University, New Haven, Connecticut.

¹ H. L. Reynolds and A. Zucker, *Phys. Rev.* **102**, 1378 (1956); M. L. Halbert and A. Zucker, *ibid.* **115**, 1635 (1959); M. L. Halbert, C. E. Hunting, and A. Zucker, *ibid.* **117**, 1545 (1960); M. L. Halbert and A. Zucker, *Nuclear Phys.* **16**, 158 (1960); A. Zucker and M. L. Halbert, *Proceedings of the Second Conference on Reactions Between Complex Nuclei, Gallinburg, Tennessee*, edited by A. Zucker, E. C. Halbert, and F. T. Howard (John Wiley & Sons, Inc., New York, 1960), p. 144.

² J. A. McIntyre, S. D. Baker, and T. L. Watts, *Phys. Rev.* **116**, 1212 (1959). E. Newman, P. G. Roll, and F. E. Steigert, *Proceedings of the Second Conference on Reactions Between Complex Nuclei, Gallinburg, Tennessee*, edited by A. Zucker, E. C. Halbert, and F. T. Howard (John Wiley & Sons, Inc., New York, 1960), p. 183.

³ H. L. Reynolds, E. Goldberg, and D. D. Kerlee, *Phys. Rev.* **119**, 2009 (1960). D. D. Kerlee, H. L. Reynolds, and E. Goldberg, *Proceedings of the Second Conference on Reactions Between Complex Nuclei Gallinburg, Tennessee*, edited by A. Zucker, E. C. Halbert, and F. T. Howard (John Wiley & Sons, Inc., New York, 1960), p. 167; J. Alster and H. E. Conzett, *ibid.*, p. 175.

⁴ Proceedings of the Conference on Reactions Between Complex Nuclei, Gallinburg, Tennessee, 1958, edited by A. Zucker, R. S. Livingston, and F. T. Howard [Oak Ridge National Laboratory Report ORNL-2606 (unpublished)]; *Proceedings of the Second Conference on Reactions Between Complex Nuclei, Gallinburg, Tennessee*, edited by A. Zucker, E. C. Halbert, and F. T. Howard (John Wiley & Sons, Inc., New York, 1960).

⁵ J. M. McKenzie and D. A. Bromley, *Phys. Rev. Letters* **2**, 303 (1959). J. M. McKenzie and D. A. Bromley, *Bull. Am. Phys. Soc.* **4**, 422 (1959). J. M. McKenzie and J. B. S. Waugh, *Proceedings of the Scintillation Counter Symposium of the Institute of Radio Engineers*, February 15, 1960 (unpublished).

⁶ D. A. Bromley, J. A. Kuehner and E. Almqvist, *Phys. Rev. Letters* **4**, No. 7, 365 (1960); *Proceedings of the Second Conference on Reactions Between Complex Nuclei*, edited by A. Zucker, E. C. Halbert, and F. T. Howard (John Wiley & Sons, Inc., New York, 1960), p. 151; *Proceedings of the International Conference on Nuclear Structure*, edited by D. A. Bromley and E. W. Vogt (University of Toronto Press, Toronto, 1960), p. 255.

⁷ E. Almqvist, D. A. Bromley and J. A. Kuehner, *Phys. Rev. Letters* **4**, 515 (1960); reference 6, p. 282 and p. 258, respectively.

⁸ N. F. Mott, *Proc. Roy. Soc. (London)* **A126** (1930).

⁹ L. E. Schiff, *Quantum Mechanics* (McGraw-Hill Book Company, Inc., New York, 1949), p. 226.

$I(2I+1)$ are antisymmetric. If the particles obey Bose-Einstein statistics the symmetric spin states are coupled with symmetric space states; if they obey Fermi-Dirac statistics, symmetric spin states are coupled with antisymmetric space states. Using this to obtain the relative weighting for symmetric and antisymmetric contributions to the differential cross section, as given by Eq. (1), results in the general expression

$$d\sigma/d\Omega = (Z^4 e^4 / 16 E^2) \{ \csc^4(\phi/2) + \sec^4(\phi/2) + [(-1)^{2I} / (2I+1)] \cdot \csc^2(\phi/2) \sec^2(\phi/2) \times \cos[\eta \ln \tan^2(\phi/2)] \}. \quad (2)$$

The Sommerfeld number η appearing in Eqs. (1) and (2) is given by

$$\eta = Z^2 e^2 / \hbar v = 0.1574 Z^2 M^{1/2} E^{-1/2}, \quad (3)$$

where M is the reduced mass in amu and E the center-of-mass energy in Mev; physically η is $\frac{1}{2}$ the ratio of the characteristic distance of closest approach given by $Z^2 e^2 / E$ and the reduced wavelength $\lambda = \hbar / Mv$.

The first two terms in Eq. (2) give the classical prediction of the scattering of identical particles while the third interference term reflects quantum mechanical aspects of the fact that the incident and target particle are not distinguishable.

From Eqs. (2) and (3) it follows that the interference term results in an oscillation about the classical predictions for both the angular distributions and the excitation functions. In the case of heavy ions this oscillation is particularly marked at low energies because of the large values of η which are involved in the argument of the cosine factor in the interference term. The Mott formulation was initially verified in part by Chadwick¹⁰ in a study of the scattering of alpha particles (~ 1 Mev) at 45° from a helium target. Further cloud-chamber measurements by Blackett and Champion¹¹ identified the interference minimum predicted by Mott⁸ at $\sim 25^\circ$. The first detailed corroboration of the Mott prediction was carried out by Heydenburg and Temmer¹² in a study of alpha-alpha scattering in the laboratory energy range $0.150 \leq E_\alpha \leq 3.0$ Mev.

In the $N^{14} + N$ measurements of Reynolds and Zucker,¹ analyzed by Porter,¹³ the energies studied were in excess of the Coulomb barrier and the experimental angular distribution data at selected energies were not in accord with the predictions of Eq. (2) because of specifically nuclear amplitudes which contributed to the measured cross section.

This paper reports measurements on both the energy and angle dependence of the differential cross section for elastic scattering of C^{12} on carbon and of O^{16} on

oxygen in the energy range from 3 to 17 Mev in the center-of-mass system. Later papers in this series will present the results on the elastic scattering of non-identical heavy ions and on studies of the associated heavy-ion reactions. A preliminary report on the latter studies on the $C^{12} + C^{12}$ and $O^{16} + O^{16}$ systems has been presented previously. Measurements also will be reported on the interference between Coulomb and resonant elastic scattering amplitudes leading to determination of the angular momenta of the entrance channel resonances observed below the barrier in the C+C reaction data.¹⁴ Studies have also been carried out on the alpha particles from the $C^{12}(C^{12}, \alpha)Ne^{20}$ reactions. Measurements on the angular distributions and excitation functions of the alpha-particle groups leading to many of the lower levels in Ne^{20} will be reported separately.

On the basis of the results obtained in all these studies a phenomenological "quasi-molecular" interaction mechanism has been suggested for the C+C system^{6,7} (analogous to that involved in a metastable homonuclear diatomic molecule). This mechanism will be discussed more fully in this and subsequent papers. The physical bases for the interaction mechanism proposed have been examined by Vogt and McManus¹⁵ and by Davis.¹⁶

EXPERIMENTAL TECHNIQUES

A. Acceleration of C^{12} and O^{16}

The measurements reported herein have been carried out with carbon and oxygen beams from the Chalk River tandem accelerator. $[C^{12}]^-$ and $[O^{16}]^-$ ions were produced by passing the positive ion beam from a standard rf source operating with CO_2 input through a hydrogen exchange cell; following selection by the injection magnet the ions were accelerated in the normal tandem fashion. Output beams were obtained of essentially equal intensity following stripping of the $[C^{12}]^-$ ions to the $[C^{12}]^{III+}$ and $[C^{12}]^{IV+}$ charge states, respectively, and of the O^{16} ions to the $[O^{16}]^{III+}$, $[O^{16}]^{IV+}$, and $[O^{16}]^{V+}$ charge states, respectively. The energy calibration and beam energy stability were determined in a previously reported series of measurements on (p, n) reactions¹⁷; beam energies in the range from 6 to 35 Mev were obtained with an energy resolution ~ 5 parts in 10^4 .

With this multiplicity of charge states in the output

¹⁴ J. A. Kuehner, B. Whalen, E. Almqvist, and D. A. Bromley, *Proceedings of the International Conference on Nuclear Structure*, edited by D. A. Bromley and E. W. Vogt (University of Toronto Press, Toronto, 1960), p. 261.

¹⁵ E. W. Vogt and H. McManus, (a) *Phys. Rev. Letters* **4**, 518 (1960); (b) *Proceedings of the Second Conference on Reactions Between Complex Nuclei, Gatlinburg, Tennessee*, edited by A. Zucker, E. C. Halbert, and F. T. Howard (John Wiley & Sons, Inc., New York, 1960), p. 297.

¹⁶ R. H. Davis, *Bull. Am. Phys. Soc.* **5**, 405 (1960); *Phys. Rev. Letters* **4**, 521 (1960); reference 15(b), p. 297.

¹⁷ D. A. Bromley *et al.*, *Can. J. Phys.* **37**, 1514 (1959).

¹⁰ J. Chadwick, *Proc. Roy. Soc. (London)* **A128**, 114 (1930).

¹¹ P. M. S. Blackett and F. C. Champion, *Proc. Roy. Soc. (London)* **A130**, 380 (1931).

¹² N. P. Heydenburg and G. M. Temmer, *Phys. Rev.* **104**, 123 (1956).

¹³ C. E. Porter, *Phys. Rev.* **103**, 674 (1956); *Phys. Rev.* **112**, 1722 (1958).

beam from the accelerator, difficulty was experienced, on occasion, in identifying the C^{12} and O^{16} beams as such. In order to establish the beam identity it was found convenient to bombard a deuterated zirconium, or deuterium gas target briefly to give either the characteristic 0.875-Mev gamma radiation from the first-excited state of O^{17} produced in the $H^2(O^{16},p)O^{17}$ reaction or the 3.086-Mev radiation from the first-excited state of C^{13} produced in the $H^2(C^{12},p)C^{13}$ reaction.

B. Beam Normalization

Even the thinnest targets used ($\sim 20 \mu\text{g}/\text{cm}^2$) were expected to be of adequate thickness to achieve complete charge equilibrium of the emergent beam independent of what incident charge state was in use. However, lack of precise knowledge of the energy variation of this equilibrium charge state precluded use of the integrated beam to give even a relative normalization of the points on an excitation curve particularly at low energies. Fortunately all targets used contained an element of sufficiently high atomic number so that the elastic scattering from it exhibited Coulomb behavior over the entire range of energies studied, at least at forward angles, and this fact was employed to normalize the energy dependence of the scattering from lighter target nuclei.

As a check on this normalization, runs were made at a few selected energies, using a thermistor bridge to measure the thermal energy flow from the beam stopper, i.e., the total power delivered by the beam instead of the beam current. The device was calibrated using proton

beams for which there are, of course, no such charge state problems. Knowing the total power arriving at the target and the energy per particle delivered by the accelerator, the particle flux incident on the target was obtained. The relative normalization of the selected points studied agreed with the more accurate normalization obtained using scattering from the high- Z target elements as noted above.

In angular distribution measurements a monitor counter fixed relative to the target and to the beam direction was used to normalize the individual measurements.

C. Detectors

All measurements reported have been made using Au-Si surface barrier detectors fabricated from 120 ohm-cm n -type Si. Units 2×2 mm and 5×5 mm in area have been operated with a bias of ~ 28 v. It has been found convenient to use a crude form of current preamplification with two stages of transistor amplification feeding the output signal through ~ 300 ft of 200-ohm cable to the accelerator control room. Two miniature hearing-aid 22.5-v dry batteries supplied all voltages for each detector system in the target area.

Use of a low-impedance input preamplifier minimizes dependence of the output signal upon the capacitance of the detector and the preamplifier input. In addition, it avoids integration of the signal at the detector and provides a very short signal pulse $\sim 30 \mu\text{sec}$ in length which minimizes overloading and resultant gain shifts in subsequent circuits at high counting rates. The signal cables were terminated in standard distributed amplifiers for use in coincidence application; in parallel, the signal was integrated using an RC network with buffering cathode followers, to provide an input suitable for double delay line linear amplifiers. Figure 1 is a schematic diagram of the system used.

Energy resolutions of between 1 and 2% were readily attainable with this system and 2×2 mm junctions; no attempt was made to improve upon this through use of thinner targets or more sophisticated circuitry. Figure 2 shows typical spectra measured with 26.5-Mev carbon and oxygen ions incident on $40\text{-}\mu\text{g}/\text{cm}^2$ carbon and $70\text{-}\mu\text{g}/\text{cm}^2$ SiO targets, respectively. It has been demonstrated generally that the junction detector outputs are linearly proportional to the energy deposited in the depletion layer independent of the specific ionization of the particle involved; it has been shown in these measurements that this linearity holds for C and O ions as well, in the energy range studied below 40 Mev. The gold electrode acts as an absorber, of course; however, this corresponds to a cutoff at less than 1-Mev C or O energy in most units. It should be noted that this electrode was an efficient absorber for optical uv and soft x radiation; this inherent insensitivity of the Au-Si units to ambient uv and soft x radiation constitutes a considerable advantage of the Au-Si relative to the diffused pn junction detectors. It should be noted, however, that

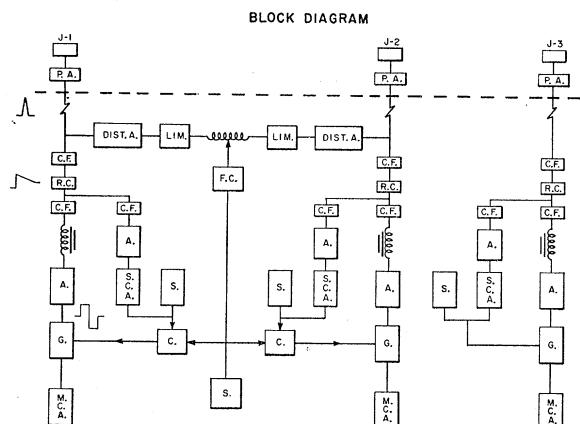


FIG. 1. Block diagram of junction detection system: The legend is as follows: P.A.—transistorized preamplifier, Dist. A.—distributed fast amplifiers, Lim—pulse limiters, F.C.—fast coincidence (~ 20 nsec) system, A.—linear amplifier (DDL), C.F.—white cathode follower, RC—pulse stretcher, SCA—single channel analyzer, G—pedestal-free gate, S—scaler, C—slow coincidence ($\sim 1 \mu\text{sec}$) system, MCA—100-channel analyzer. The circuit shown allows self-gating of any of the detector outputs to facilitate the setting of pulse gates on particular spectrum peaks. The two junction detectors shown on the left are mounted rigidly at 90° to each other in the scattering plane for coincidence studies as shown in Fig. 3.

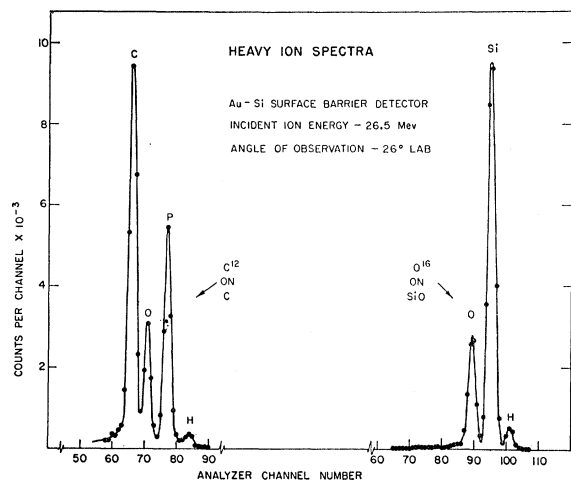


FIG. 2. Typical pulse height spectra observed using Au-Si junctions and the system shown in Fig. 1. Peak identification is discussed in the text.

the apparent cutoff at heavy-ion energies ≤ 1 Mev could in part at least reflect partial recombination at the ends of the ionization columns in the detectors. No careful study of this phenomenon was attempted.

Several individual Au-Si detectors have been in use over periods of 10–15 months; no observable changes in their characteristics have been found after, in some cases, up to 10^{13} heavy-ion counts. Indeed it has been observed that the Au-Si unit characteristics show slight improvement with aging. This presumably reflects the fact that the surface states responsible for the surface barrier operation reach an equilibrium density following further oxidation and that normal ambients tend to

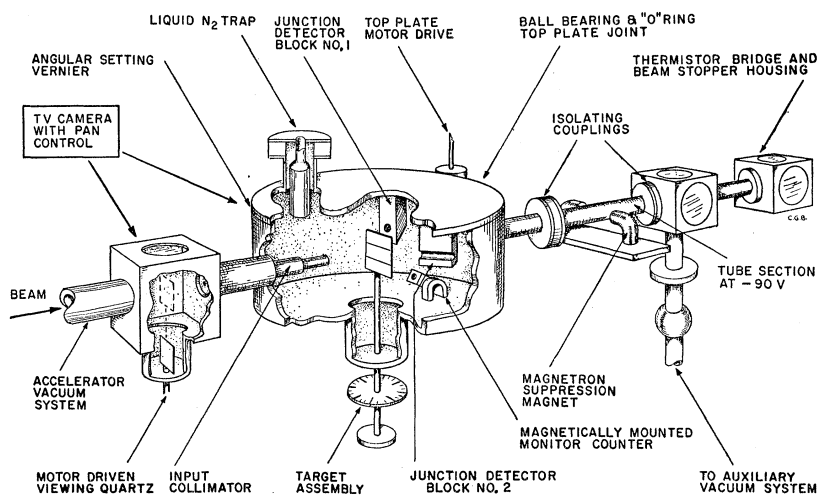
produce a *p*-type surface on the *n*-type base Si increasing the surface resistivity and decreasing the surface leakage. The opposite effect, wherein the ambients change the surface of the *p*-type material normally used in the base wafers of the *p-n* diffused junctions to *n* type of lower resistivity may explain the more rapid observed deterioration of the characteristics of these detectors.

In obtaining the excitation curves three detectors were used and their outputs displayed simultaneously on three 100-channel Goulding analyzers¹⁸; in obtaining the angular distributions the outputs of two movable counters were displayed simultaneously as 100-channel spectra and a voltage window was set to record the corresponding number of events in the elastic peak in the fixed-angle monitor detector spectrum.

In order to make certain the identification of the O^{16} +oxygen elastic scattering events at the highest energies studied, use has been made of the well known fact that for elastic scattering of identical particles, the separation angle, in the laboratory system, between the scattered and recoil moments is uniquely fixed at 90° independent of the scattering angle. Two detectors rigidly fixed at 90° to one another in the scattering plane were used in coincidence to reject all but true coincidence events wherein the scattered and recoil ions were detected simultaneously. A relatively long coincidence resolving time of 1 to 2 μ sec was adequate in these measurements since the coincidence efficiency was $\sim 100\%$.

In obtaining the angular distribution the two detectors mounted rigidly at 90° to one another were used simultaneously to give two points on the angular distribution on opposite sides of the zero angle.

FIG. 3. Schematic illustration of the detection system in use. The top plate of the chamber is supported on an array of captive ballbearings and the associated vacuum seal is obtained using a standard O-ring. The target system permitted simultaneous assembly of more than one target, e.g., a gold calibration target together with the target under study and in some instances a calibration radioactive alpha particle source as well. Initial alignment of the chamber was accomplished optically on the beam line of sight as determined by an alignment telescope rigidly mounted on the primary 90° beam bending magnet of the accelerator. Preamplifiers were mounted outside the chamber and the connections to the detectors brought out through Kovar seals. The TV camera could be focused on a viewing quartz at the entrance of the collimator system to facilitate adjustment of beam steering and focusing elements or on the angular position vernier on the chamber top carrying the detectors.



¹⁸ F. S. Goulding, *Multichannel Pulse-Height Analysis*, National Academy of Science, National Research Council Publication No. 467 (National Research Council, Washington, D. C., 1956), p. 86.

D. Targets

Self-supporting carbon targets were prepared using a slight modification of a previously reported evaporation technique.¹⁹ In order to obtain uniform, very thin targets it was found advisable to lay down the Alconox stripping film, prior to the carbon evaporation, by spraying a polished glass plate, heated to 150°C, with a fine airborne mist of the Alconox solution in distilled water. Following thorough drying of the resultant uniform stripping film, the supporting plate was mounted to allow evaporation of the carbon film either from a vacuum arc between graphite electrodes or from a graphite rod heated by passing an electric current through it. Films of controlled thicknesses were obtained by varying the power input and/or the exposure time. The carbon films were then stripped in a heated, distilled-water bath to which a few percent of acetone or insulin was added to decrease the surface tension. (Self-supporting targets ~ 1 cm in diameter and 20–150 $\mu\text{g}/\text{cm}^2$ thick were prepared in this way.)

All targets prepared in this way had a significant oxygen contaminant which varied from target to target but which was quite stable under bombardment. Significant phosphorous contamination remained from the stripping film used; however, since this provided a convenient calibration peak throughout the measurements no serious attempt was made to eliminate it.

A number of possible oxygen targets were examined for use with heavy ions. In particular it was found that Al_2O_3 targets fabricated, using a previously reported technique,²⁰ in the nominal range of thickness from 350 to 1000 Å were sufficiently nonuniform to prevent the separation of elastic scattering events from the different target nuclei using pulse height selection alone. Microscopic examination of these targets showed a fine striated film structure which presumably results in the observed decrease in resolution. Targets prepared by oxidizing micro-inch nickel foil in an oxygen atmosphere using the focused output from a high-temperature carbon arc²¹ were unsuitable because the strong elastic scattering from the Ni made extraction of the lower energy, lower intensity elastically scattered group from oxygen very difficult. Successful targets were prepared using evaporated SiO and a technique identical to that just described for the carbon targets. Self-supporting targets 1 cm in diameter and ~ 100 $\mu\text{g}/\text{cm}^2$ thick were prepared in this way.

Target thicknesses were determined both by direct weighing of film sections and by comparison of the yield of elastically scattered heavy ions at low energies with that calculated assuming pure Coulomb scattering. In terms of energy loss the carbon targets are estimated

to be < 100 keV and those of SiO ~ 250 keV in the center-of-mass system.

E. Scattering Chamber

An existing chamber with an evacuated volume 12 in. in diameter \times 6 in. deep, originally designed for precision proton scattering measurements with gas targets,²² was modified for use with the junction detectors. The beam on target was defined by a series of four $\frac{1}{8}$ -in. diameter collimating apertures. Three Au-Si detectors were mounted rigidly to the rotatable lid of the chamber, two of these at exactly 90° to one another for use in coincidence studies of elastic scattering of identical particles. (This feature was required only in the O^{16} on oxygen studies at the highest energies involved.) A fourth detector was mounted for use as a fixed monitor counter; since the Au-Si detectors are unaffected by magnetic fields, it was convenient to use a small Alnico V horseshoe magnet as the base for this mount, thus permitting simple attachment at any desired location on the walls of the steel scattering chamber. A schematic view of this system is shown in Fig. 3.

Collimating apertures were fitted to each of the detectors. In the angular distribution measurements, angular apertures of 0.3° were used, corresponding to a solid angle of 6×10^{-6} of a sphere; in the excitation curve measurements the solid angles were increased to 2×10^{-4} of a sphere.

Following traversal of the chamber, the ion beam passed through an insulated section of tubing (maintained at 90 v negative relative to the beam system) with a transverse magnetic field applied with a permanent magnetron magnet to suppress electron transmission, and was finally stopped in a gold plate connected to the beam integrator and to the thermistor bridge. Two separate diffusion pump stations were provided on the target line together with a large liquid N_2 trap in the scattering chamber itself in order to minimize the amount of residual gas present; without these, beam current measurements were unreliable.

Use of successive magnetic elements to steer and focus the beam onto the target, as was the case here, poses particular problems when accelerating heavy ions. Following energy analysis in the main 90° deflecting magnet, the heavy-ion beam traverses some 35 ft of vacuum line and a quadrupole lens system before reaching the scattering chamber. As a result of interactions with the residual gas in the vacuum line, some beam ions undergo charge exchange and are defocused because the lens system (with markedly different focal lengths for the different charge states) focuses only a single charge component of the monoergic set on target. With the pumping and trapping system described, a pressure $\sim 5 \times 10^{-5}$ mm Hg was obtained in the target

¹⁹ D. A. Bromley *et al.*, Phys. Rev. **105**, 957 (1957).

²⁰ D. A. Bromley, J. A. Kuehner, and E. Almqvist, Nuclear Phys. **13**, 1 (1959).

²¹ H. Holmgren, *et al.* Rev. Sci. Instr. **25**, 1026 (1954); T. F. Stratton *et al.* Phys. Rev. **98**, 629 (1955).

²² A. J. Ferguson, R. L. Clarke, and H. E. Gove, Phys. Rev. **115**, 1655 (1959).

line and at this pressure the charge exchange loss was negligible.

F. Procedure

The alignment of the scattering chamber was checked by examining the elastic scattering of 27-Mev oxygen ions from a gold leaf target. The results are shown in Fig. 4 where the solid line passing through the points is the Rutherford prediction. The angular zero for each of the movable detectors was determined by making measurements on the rapidly falling elastic scattering angular distribution at positive and negative forward angles, as well as from examination of the symmetric maximum at $\theta_{\text{lab}}=45^\circ$ in the scattering of identical particles. An external vernier arrangement permitted setting angles to within 0.1° .

As a result of the rapid variation of the energy and yield of the elastically scattered ions with the angle of observation, identification of the groups scattered from different target contaminants posed a particular problem. From the elastic scattering kinematics in the case of C^{12} bombardment of one of the carbon targets used it follows simply that the laboratory energies of the carbon ions elastically scattered from the C^{12} , O^{16} , and P^{31} target nuclei are given by

$$E^{\text{C}}(\theta) = E_0^{\text{C}} \cos^2\theta, \quad (4)$$

$$\{E^{\text{O}}(\theta)\}^{\frac{1}{2}} = 0.428\{E_0^{\text{C}}\}^{\frac{1}{2}} \cos\theta \pm \{0.143E_0^{\text{C}} + 0.183E_0^{\text{C}} \cos^2\theta\}^{\frac{1}{2}}, \quad (5)$$

$$\{E^{\text{P}}(\theta)\}^{\frac{1}{2}} = 0.279\{E_0^{\text{C}}\}^{\frac{1}{2}} \cos\theta \pm \{0.442E_0^{\text{C}} + 0.078E_0^{\text{C}} \cos^2\theta\}^{\frac{1}{2}}, \quad (6)$$

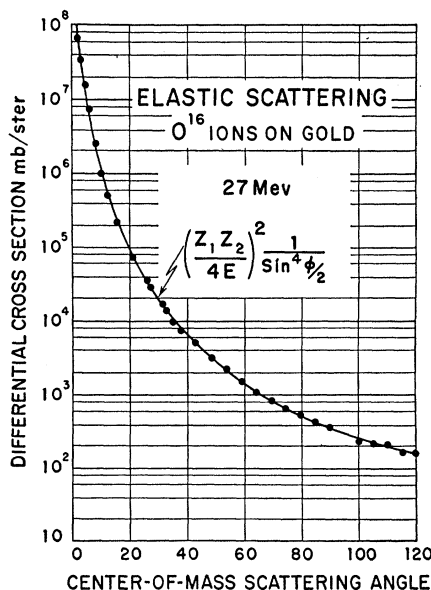


FIG. 4. Alignment check using Coulomb scattering of O^{16} ions in gold. The solid curve is the theoretically predicted differential cross section.

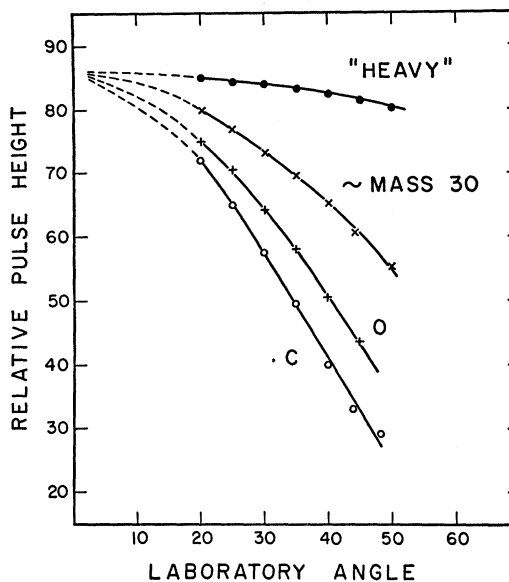


FIG. 5. Typical kinematic plot for elastic scattering of C^{12} on carbon targets.

where E_0^{C} is the laboratory energy of the incident C^{12} ions. In analyzing the experimental data it has been convenient to use plots such as that shown in Fig. 5 to follow the individual elastically scattered groups with changing angle of observation.

All experimental data have been converted to the center-of-mass system for presentation herein. In the case of elastic scattering of identical particles as considered here, this transformation is particularly simple in that the angles, intensities, and energies are related by

$$\phi_{\text{c.m.}} = 2\theta_{\text{lab}}, \quad (7)$$

$$I_{\text{c.m.}} = \frac{1}{4} \sec\theta_{\text{lab}} I_{\text{lab}}, \quad (8)$$

$$E_{\text{c.m.}} = \frac{1}{2} E_0^{\text{C}}. \quad (9)$$

The indistinguishability of the scattered and recoil particles implies symmetry relative to $\phi_{\text{c.m.}}=90^\circ$ in all angular distributions. In all cases measurements were continued beyond this angle to demonstrate that the symmetry requirement was fulfilled; this served simply as a check on systematic errors. In the only previously reported study of the elastic scattering of identical heavy ions ($\text{N}^{14} + \text{N}^{14}$) such a systematic error did appear,¹² and only at the highest energy studied was a symmetric angular distribution found; as will be apparent in later figures, symmetric results have been obtained in the data presented here.

RESULTS

Figure 2 shows a typical spectrum measured for 26.5-Mev C^{12} ions on a $40\text{-}\mu\text{g}/\text{cm}^2$ carbon target. As noted previously, the resolution inherent in the Au-Si detectors and the tandem accelerator beam made it

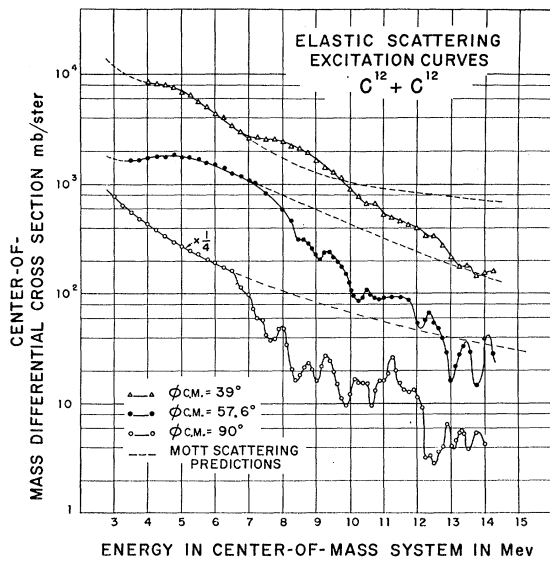


Fig. 6. Excitation curves for the elastic scattering of C^{12} on C^{12} . The dashed curves are the Mott scattering predictions at the indicated angles. The 90° data, and prediction have been multiplied by a 0.25 scale factor for display purposes here.

possible to resolve the groups of C^{12} ions elastically scattered from the various target components and incidentally from inelastically scattered groups. Consequently it has not been necessary to use the more elaborate coincidence techniques in the carbon-on-carbon measurements.

Figure 6 shows the elastic scattering excitation curves measured in the laboratory energy range from 6 to 28 Mev corresponding to the center-of-mass range from

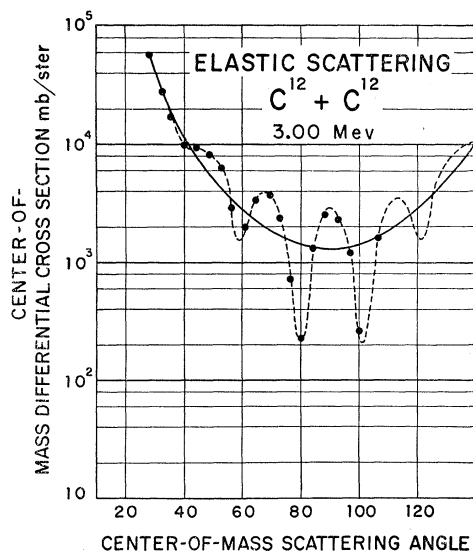


Fig. 7. Elastic scattering angular distribution for $C^{12}+C^{12}$ at $E_{c.m.} = 3.00$ Mev. The solid curve is the Rutherford prediction; the dashed curve is the Mott prediction. The spot diameters encompass the statistical counting errors.

3 to 14 Mev. Each of these curves represents the results of three separate consistent measurements. The relative statistical errors are encompassed in the spot diameters. The dashed curves show in each case the cross section dependence predicted by Eq. (2) for Mott scattering.

It should be noted that only in the case of $\theta_{lab} = 45^\circ$ does the Mott expression [Eq. (2)] predict the same E^{-2} energy dependence of the differential cross section as does the classical expression. This results from the fact that at $\phi = 90^\circ$, $\ln \tan^2(\phi/2) = 0$ and $\cos[\eta \ln \tan^2(\phi/2)] = 1$, independent of η hence E . Since the shapes both of these excitation curves and of the angular distributions to follow are in accord with the Mott scattering predictions for energies below the Coulomb barrier, the cross-section scale on the ordinate of the figure has been adjusted to give agreement with the predicted Mott cross-section values at low energies.

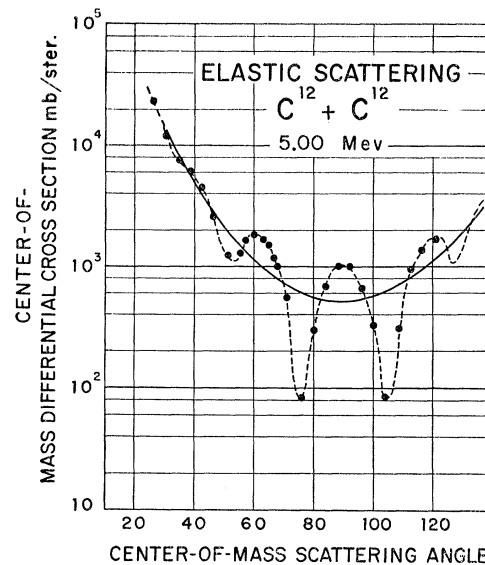


Fig. 8. Elastic scattering angular distribution for $C^{12}+C^{12}$ at $E_{c.m.} = 5.00$ Mev. See caption to Fig. 7.

The absolute differential cross-section values which were measured here are in accord with this adjustment but have an estimated possible error by a factor of 2 reflecting uncertainties in the target thickness and beam flux measurements.

Angular distributions of C^{12} ions elastically scattered from carbon are shown in Figs. 7-12 for center-of-mass energies of 3.00, 5.00, 10.00, 11.25, 12.50, and 13.35 Mev, respectively. In each case the light full line is the classical Rutherford prediction and the dashed line the corresponding Mott prediction; the experimental points are the solid circles and the relative normalization in each case is taken from the 90° yield curve of Fig. 4. The heavy curves shown at energies above the Coulomb barrier are simply drawn to connect the experimental points.

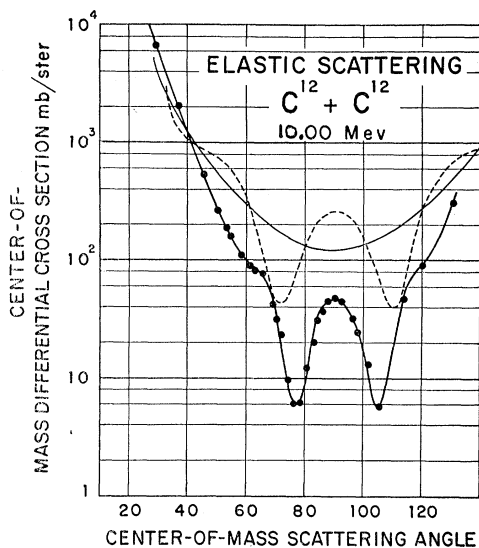


FIG. 9. Elastic scattering angular distribution for $C^{12}+C^{12}$ at $E_{c.m.}=10.00$ Mev. See caption to Fig. 7.

Figure 13 presents corresponding excitation curves for the $O^{16}+O^{16}$ system at three angles of observation. Here again the dashed curves are the Mott predictions; the oscillation about the classical E^{-2} dependence is more striking than in the $C^{12}+C^{12}$ case because of the higher η values involved.

Figures 14-18 present angular distributions of elastically scattered O^{16} ions measured at center-of-mass energies of 7.0, 8.8, 10.0, 13.0, and 15.0 Mev, respectively. Here the light solid line is the classical prediction, the dashed line the Mott prediction (except at the lowest energies where it is covered by the experimental data), and the heavy line is drawn to join the experi-

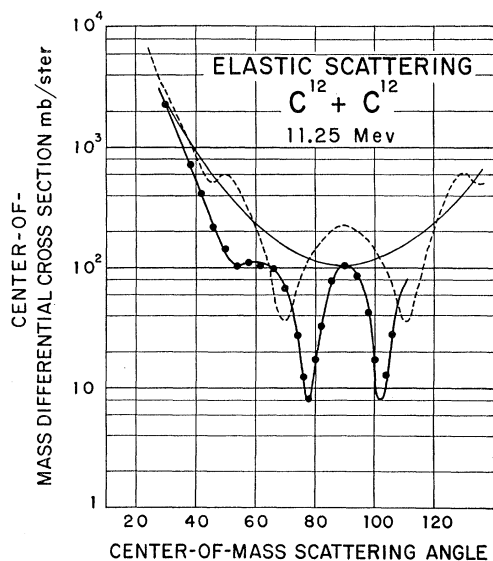


FIG. 10. Elastic scattering angular distribution for $C^{12}+C^{12}$ at $E_{c.m.}=11.25$ Mev. See caption to Fig. 7.

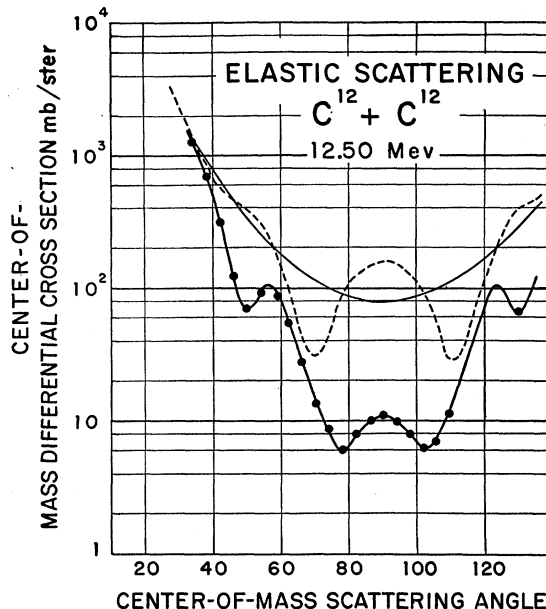


FIG. 11. Elastic scattering angular distribution for $C^{12}+C^{12}$ at $E_{c.m.}=12.50$ Mev. See caption to Fig. 7.

mental points. Relative normalization has been taken from the 90° excitation curve of Fig. 13.

Much more detailed excitation function measurements¹⁴ have been carried out in the region of the Coulomb barrier for both the $C+C$ and $O+O$ systems. These data will be reported separately where interference fluctuations in these elastic cross sections²³ will be used to determine the angular momenta of the

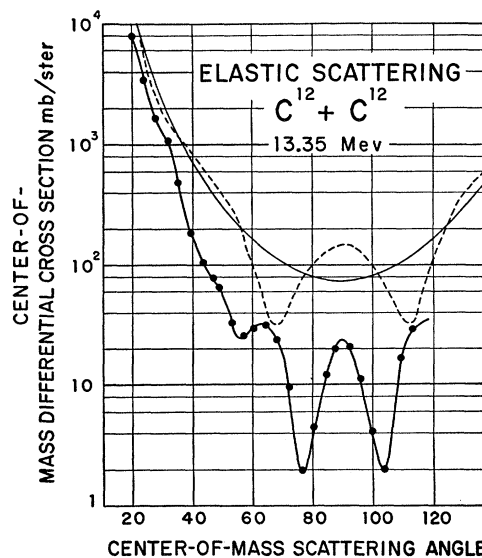


FIG. 12. Elastic scattering angular distribution for $C^{12}+C^{12}$ at $E_{c.m.}=13.35$ Mev. See caption to Fig. 7.

²³ J. M. Blatt and L. C. Biedenharn, *Revs. Modern Phys.* 24, 258 (1952).

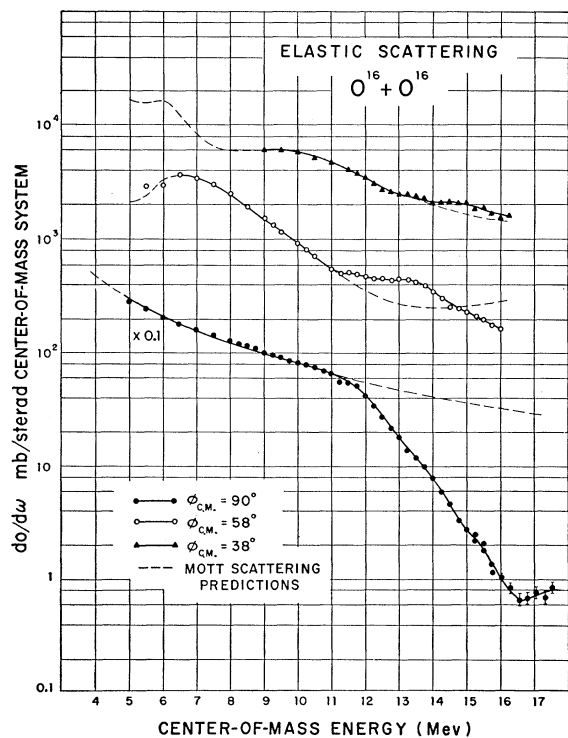


FIG. 13. Excitation curves for the elastic scattering of $O^{16}+O^{16}$. The dashed curves are the Mott predictions at the indicated angles. The 90° data and prediction have been multiplied by a 0.1 scale factor for display purposes here.

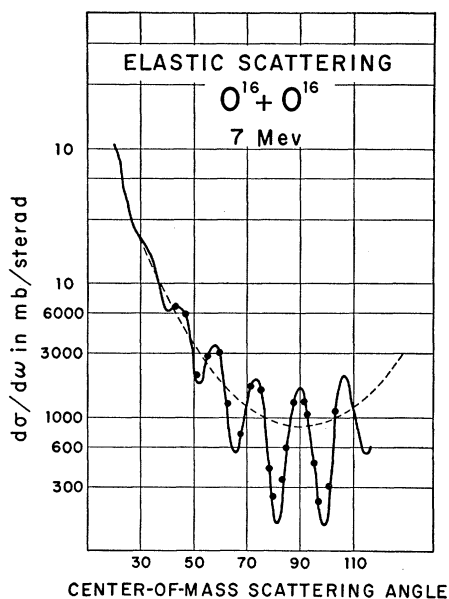


FIG. 14. Elastic scattering angular distribution for $O^{16}+O^{16}$ at $E_{c.m.}=7$ Mev. The dashed curve is the Rutherford prediction and the solid curve the Mott prediction for the differential cross section. The spot diameter encompasses the statistical counting errors.

entrance channel resonances found in the C+C reaction studies⁷ at energies just below the Coulomb barrier.

DISCUSSION

A. General

The striking and unexpected feature of the yield curves in Fig. 6 is of course the prominent structure in the curves measured at $\phi_{c.m.}=57.6^\circ$ and 90° . For $\phi_{c.m.}=90^\circ$ for example, the differential cross section changes by an order of magnitude in going from 11.25 to 12.25 Mev in the center of mass. Moreover, some of the structure shows widths <200 kev equal to the effective target thickness in use, demonstrating that states having surprisingly long lifetimes $>10^{-21}$ sec are involved. The fact that the structural details of

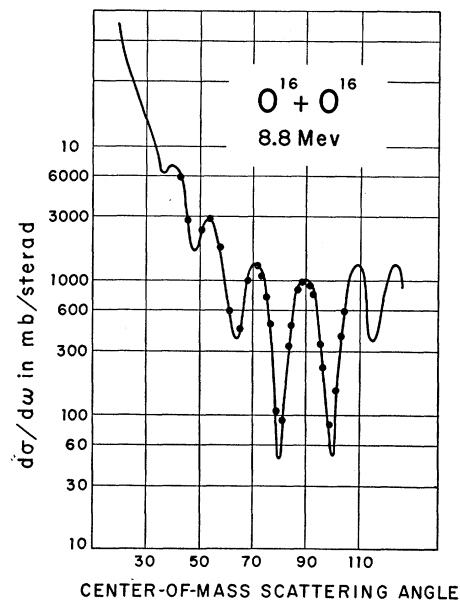


FIG. 15. Elastic scattering angular distribution for $O^{16}+O^{16}$ at $E_{c.m.}=8.8$ Mev. The solid curve is the Mott scattering prediction.

these curves are not correlated at different angles of observation implies an interference explanation involving the compound elastic decay amplitudes for these states and the normal Coulomb amplitudes. The energy range studied corresponds to excitations in the range 17 to 28 Mev in the Mg^{24} compound system using the atomic mass values given by Kravtsov.²⁴

Experimental data thus far reported on heavy ion induced reactions have shown that a statistical model gives a satisfactory accounting for the energy spectra of emitted nucleons and light fragments. These explanations assume formation of a compound system following coalescence of the projectile and target nuclei with subsequent sharing of the available excitation energy among the nuclear degrees of freedom in accordance

²⁴ V. A. Kravtsov, *Uspekhi Fiz. Nauk.* 65 (3), 451 (1958).

with the laws of statistical mechanics. Because of the very large number of these degrees of freedom, hence levels in the compound system, it would be anticipated that at excitations in the range studied here the level density would be sufficiently high to insure complete averaging over the individual resonances to give a smoothly varying excitation curve. Moreover, in terms of a compound nucleus picture, the probability of having a true compound elastic decay of the compound state involving reformation of the C^{12} nuclei in their ground states and their re-emission in the entrance channel would be expected to be extremely small. Very rough qualitative estimates suggest a branching ratio for this decay mode $\sim 0.1\%$. The carbon results shown in Fig. 6 are consistent with neither of these expectations, suggesting that a different mechanism is involved.

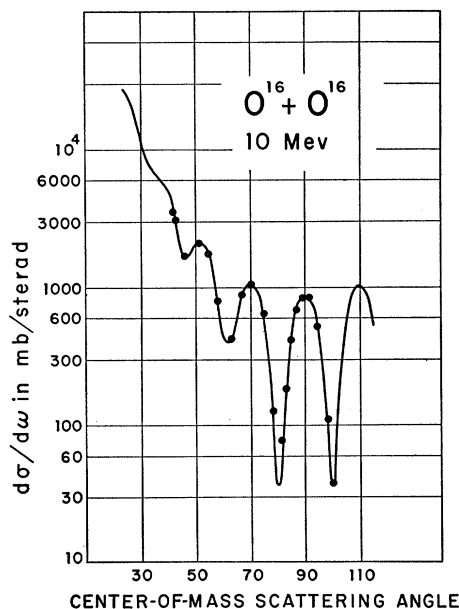


FIG. 16. Elastic scattering angular distribution for $O^{16}+O^{16}$ at $E_{c.m.} = 10$ Mev. The solid curve is the Mott scattering prediction.

In contrast, the excitation curves for the $O^{16}+O^{16}$ system show no resonant structure and thus are consistent with a compound system mechanism. Above the Coulomb barrier these excitation curves show the roughly exponential decrease in differential cross section with energy which has characterized almost all of the alpha, deuteron, and heavy-ion scattering data reported previously.⁴ This decrease is, however, different from those previously observed in that after continuing down for roughly a factor of 100 it terminates abruptly at $E_{c.m.} \sim 16.5$ Mev and $(d\sigma/d\Omega)_{90^\circ} \sim 10$ mb/sr. Further discussion of this phenomenon will be presented later in this paper. The region of excitation in the compound system S^{32} covered in these measurements is from 21.5 to 34.0 Mev.

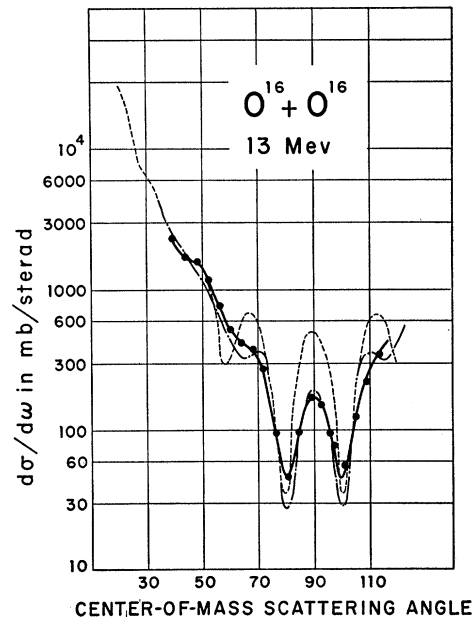


FIG. 17. Elastic scattering angular distribution for $O^{16}+O^{16}$ at $E_{c.m.} = 13$ Mev. The dashed, broken, and solid curves are the Mott and Blair predictions and the experimental data, respectively. In the latter case the curve is simply drawn through the experimental points; the Blair predictions correspond to a cutoff l_{max} value of 6 as given from a semi-classical turning point argument.

B. Interaction Radii

In previous preliminary reports on these data⁶ the quarter-point method suggested by Blair²⁵ was used as

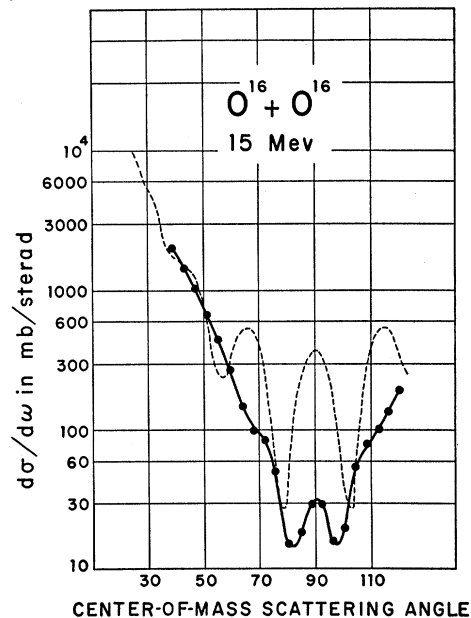


FIG. 18. Elastic scattering angular distribution for $O^{16}+O^{16}$ at $E_{c.m.} = 15$ Mev. The dashed curve is the Mott prediction and the solid curve has been drawn through the experimental points.

²⁵ J. S. Blair, Phys. Rev. **95**, 1218 (1954); *ibid.* **108**, 827 (1957).

TABLE I. Reduced reaction radii r_0 for the $C^{12}+C^{12}$ system in fermis.

Extraction recipe	$\phi_{e.m.} = 90^\circ$		$\phi_{e.m.} = 57.6^\circ$		$\phi_{e.m.} = 39^\circ$	
	Linear	Average	Linear	Average	Linear	Average
Crossover point	1.80	1.68	1.75	1.58	1.68	1.54
Quarter point	1.75	1.61	1.77	1.57	1.72	1.59

a systematic and consistent method for the extraction of an interaction radius for each of the systems studied. Kerlee, Blair, and Farwell²⁶ have shown that this quarter-point recipe is considerably inferior, in its precision, to a second semiclassical recipe which they suggest based on the location of a crossover on plots of $(d\sigma/d\Omega)/(d\sigma/d\Omega_{\text{Coul}})$ as a function of l_{max}/η for variable η .

Subsequent to the early reports on this work,^{6,7} the excitation curve data have been re-analyzed using this crossover point recipe. In the case of the C+C data it was found that the radii obtained were quite sensitive to the assumptions made regarding the treatment of the resonant structure.

Table I lists the reduced interaction radius r_0 , defined by

$$\begin{aligned} R_{\text{int}} &= r_0(A_1^{\frac{1}{3}} + A_2^{\frac{1}{3}}) \\ &= 2r_0A^{\frac{1}{3}} \text{ for identical-particle systems, obtained for the C+C system at three angles of observation.} \end{aligned} \quad (10)$$

In each entry the larger number was obtained from linear extrapolation of the excitation curve at energies below the onset of resonance structure and the smaller from an average curve constructed through the resonant structure. Since the resonant structure predominantly results from the interference between the resonant and Coulomb amplitudes, the latter averaging process is presumably the more realistic.

From the $\phi = 90^\circ$, $O^{16}+O^{16}$ data, $r_0 = 1.66$ f is obtained using the crossover recipe and $r_0 = 1.62$ f from the quarter-point recipe. Consequently this analysis suggests that there is no significant difference between the interaction radii for the C+C and O+O systems as deduced from the elastic excitation curves. This supersedes the earlier analysis⁶ which used linear extrapolation of the excitation curve to give the larger radius for the C+C system.

C. Excitation Curves and Angular Distributions

As shown in Figs. 6–8, 13–16 for energies below the Coulomb barrier, both the excitation curves and the angular distributions are in good accord with the Mott scattering predictions; both clearly show the oscillation about the classical predictions resulting from the interference term in Eq. (2).

At energies above the Coulomb barrier, both the

²⁶ D. D. Kerlee, J. S. Blair, and G. W. Farwell, Phys. Rev. **107**, 1343 (1957).

excitation curves and the angular distributions near 90° in the center-of-mass system show the characteristic decrease in cross section below the Mott predictions; this decrease has been fitted in many instances by the Blair model or one of its many refined or modified versions.^{26–28} In its simplest or “sharp-cutoff” form this model is based on the assumption of a well-defined interaction radius, total nuclear absorption of all partial waves in the incident beam with corresponding classical trajectories passing within this radius, and pure Coulomb scattering of all partial waves with trajectories passing outside of this radius. The cutoff orbital angular momentum l_{max} is obtained from a semiclassical turning-point argument by equating the incident energy to the sum of the Coulomb and centrifugal barriers, i.e.,

$$E = [Z^2e^2/R_{\text{int}}] + [l_{\text{max}}(l_{\text{max}}+1)\hbar^2/2M(R_{\text{int}})^2], \quad (11)$$

where M is the reduced mass of the system and E the energy in the c.m. system.

The abrupt transition assumed between the absorption and scattering is reflected in spurious diffraction oscillations in the model predictions; these have been reduced using various *ad hoc* techniques. The most elegant published refinement is that due to McIntyre *et al.*,²⁸ suggested by calculations of Cheston and Glassgold,²⁹ wherein a smooth transition between absorption and scattering is obtained over a range of l values and in addition the phases of the partial waves undergo a smooth modification in this region. Austern and co-workers³⁰ have recently carried out a more detailed investigation of these phenomena obtaining more rigorous predictions for the absorption and scattering behavior particularly in the region of cutoff.

For discussion purposes herein only the simpler “sharp-cutoff” formulation is used in an attempt to obtain a qualitative understanding of the gross features observed. For identical spin-zero bosons, the Blair model expression for the differential elastic scattering is given by

$$\begin{aligned} d\sigma/d\Omega &= (Z^4e^4/16E^2) \left| \csc^2(\phi/2) \exp[-i\eta \ln \sin^2(\phi/2)] \right. \\ &\quad \left. + \sec^2(\phi/2) \exp[-i\eta \ln \cos^2(\phi/2)] \right. \\ &\quad \left. + \frac{2}{i\eta} \sum_{l=0}^{l_{\text{max}}} (2l+1) \exp(2i\delta_l) P_l(\cos\phi) \right|^2, \end{aligned} \quad (12)$$

where all quantities are in the center-of-mass system,

²⁷ N. S. Wall, J. R. Rees, and K. W. Ford, Phys. Rev. **97**, 726 (1953).

²⁸ J. A. McIntyre, K. H. Wang, and L. C. Becker, Phys. Rev. **117**, 1337 (1960); J. A. McIntyre, S. D. Baker, and K. H. Wang, reference 15(b), p. 180; J. A. McIntyre, K. H. Wang, and S. D. Baker, *Proceedings of the International Conference on Nuclear Structure*, edited by D. A. Bromley and E. W. Vogt (University of Toronto Press, Toronto, 1960), p. 384.

²⁹ W. B. Cheston and A. E. Glassgold, Phys. Rev. **106**, 1215 (1957).

³⁰ N. Austern, reference 14, p. 323.

and in addition to the definitions following Eqs. (1), δ_l is the Coulomb phase shift defined as

$$\delta_l = \sigma_l - \sigma_0 = \sum_{k=1}^l \tan^{-1}(\eta/k), \quad (13)$$

$$\sigma_l = \Gamma(l+1+i\eta)/\Gamma(l+1-i\eta). \quad (14)$$

The restriction to identical zero-spin nuclei implies that only even l values are permitted in Eq. (12); this considerably simplifies the computation of angular distribution over previously reported situations, i.e., $N^{14}+N^{14}$ where both even and odd orbital momenta are allowed.¹³

It has been demonstrated in many systems^{25,26} that if η is large, the formalism of Eq. (12) predicts excitation curves of the type measured for $O^{16}+O^{16}$ over a limited energy range near the top of the Coulomb barrier. It has similarly been found possible to obtain quite adequate fits to the $O^{16}+O^{16}$ elastic scattering angular distributions at energies in the region of the barrier; the low cross section for elastic scattering at $E_{c.m.} \sim 16.5$ Mev requires very long runs to obtain a corresponding angular distribution and this has not yet been measured. Figure 17 for example compares the differential cross section as calculated from Eq. (12) with $l_{max}=6$ with the experimental data measured at $E_{c.m.} = 13$ Mev. The

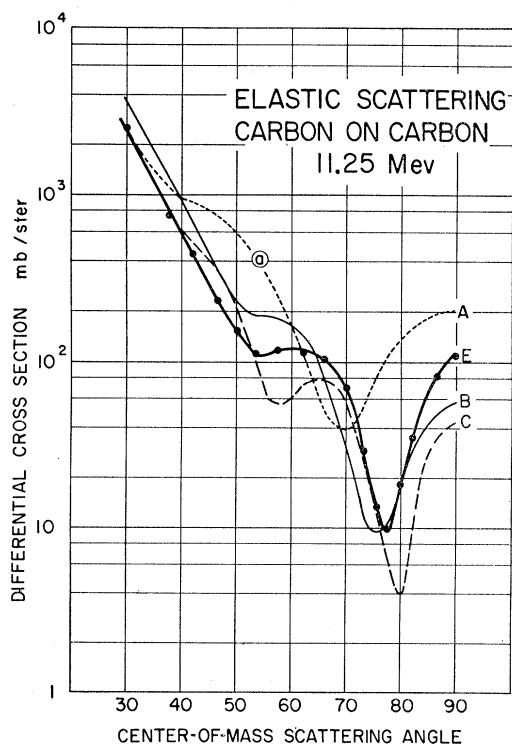


FIG. 19. Blair Model calculations of the $C^{12}+C^{12}$ elastic angular distribution at $E_{c.m.} = 11.25$ Mev. Curves A, E, B and C are, respectively, the Mott predictions, the experimental data, the Blair prediction for $l_{max}=4$, and a Blair prediction for $l_{max}=6$.

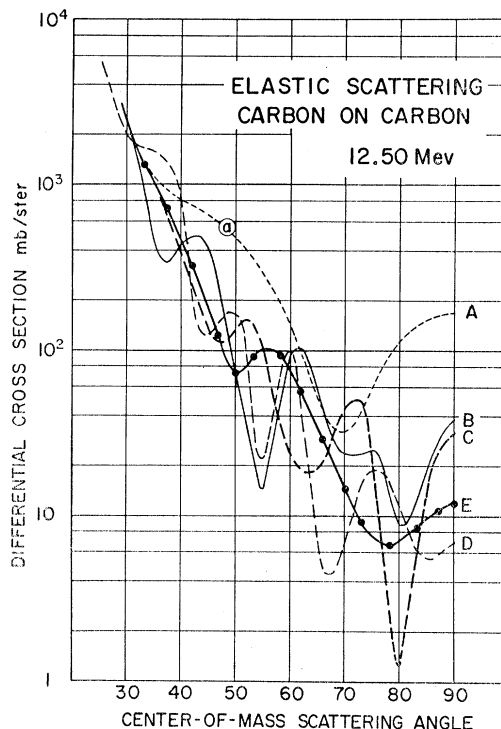


FIG. 20. Blair Model calculations of the $C^{12}+C^{12}$ elastic angular distributions at $E_{c.m.} = 12.50$ Mev. Curves A and E are the Mott predictions and experimental data, respectively; curve C is Blair prediction corresponding to $l_{max}=8$, while curves B and D correspond to resonant absorption of high partial waves as discussed in the text.

value of $l_{max}=6$ is that obtained semi-classically from Eq. (11) and does, in fact, give much better fit than either of the adjacent allowed values of $l_{max}=4$ or 8.

Equation (12) has also been evaluated for the $C^{12}+C^{12}$ system; typical results are shown in Figs. 19 and 20. In Fig. 19, corresponding to $E_{c.m.} = 11.25$ Mev, the characteristic sharpening of the lowest minimum and its displacement toward 90° relative to the Mott predictions are apparent. The curves labeled B and C correspond to Eq. (12) with $l_{max}=4$ and 6, respectively, and qualitatively bracket the experimental data. It should be noted however that Eq. (11) predicts a cutoff l value of 10 at this energy; the corresponding calculation shows no agreement with the data.

Figure 20 compares experiment and calculations at $E_{c.m.} = 12.50$ Mev at the sharp minimum in the excitation curve of Fig. 5. In this case it was found that no permitted cutoff value $l_{max} \leq 16$ gave even qualitative agreement with the data. Curve C in the figure is typical of these calculations and corresponds to $l_{max}=8$.

In view of the marked resonant structure in the excitation curve of Fig. 6 it appeared possible that angular distributions such as that of Fig. 11 might reflect a situation involving resonant absorption of a particular incident partial wave. If this resonant wave corresponds to a grazing collision with $l_r > l_{max}$ it be-

comes possible to carry out a Blair model calculation wherein complete nuclear absorption is assumed for l_r as well as for all $l \leq l_{\max}$. Such calculations have been carried out and curves *B* and *D* in Fig. 20 correspond to situations where $l_r = l_{\max} + 4$ for $l_{\max} = 4$ and 6, respectively. As shown, no quantitative fit is obtained; however, discounting in part the oscillatory behavior characteristic of the sharp-cutoff approximation used, the qualitative agreement obtained is much superior to that for a simple l_{\max} cutoff alone. This lends credence to the assumption that the sharp resonant structure of Fig. 6 reflects the capture of selected, high-order partial waves to form high-spin compound states of relatively long life. No further significance should be attached to Fig. 20.

The fact that the angular distributions for the $C^{12} + C^{12}$ system shown in Figs. 11 and 12 do not change monotonically with energy in contrast to those for the $O^{16} + O^{16}$ system shown in Figs. 16–18 which do, is also in accord with this hypothesis and suggests resonant effects in the former.

D. Diffraction Effects

It should be noted here that an *a priori* possible explanation for the structure in the data of Fig. 6 follows from the observation of diffraction structure in heavy-ion elastic scattering angular distribution studies. When such structure is present in the angular distributions, an excitation curve measured at a fixed angle of observation will show quasi-resonant structure corresponding to the movement of the diffraction extrema over the fixed counter aperture as changing kinematics and changing angular momenta compress or expand the features of the angular distributions. An analysis of much of the available elastic scattering data² has resulted in the empirical correlation that diffraction structure is present when $\eta \leq 5$ and not present when $\eta > 5$. This correlation can be shown to be qualitatively consistent with a modified Blair model.²⁸

Since the energy range studied here in the $C^{12} + C^{12}$ system corresponds to $7.4 \geq \eta \geq 3.7$ and in the $O^{16} + O^{16}$ system to $12.8 \geq \eta \geq 6.8$, it would be expected on this basis that diffraction structure should be present in the $C^{12} + C^{12}$ excitation function but not in that for $O^{16} + O^{16}$. To investigate this effect, a calculation based on the Blair sharp-cutoff model²⁵ has been made for the 90° excitation function for $C^{12} + C^{12}$. Since Eqs. (11) and (12) are defined only for discrete energies a modification has been used which has allowed the cross section to be defined continuously. Instead of a sharp cutoff in l , a transition region of width $2l$ has been defined in which the influence of that partial wave which lies inside varies continuously from zero to its maximum value. This modification was chosen to affect the sharp-cutoff assumption least and still allow a meaningful definition. In this modification an additional factor has

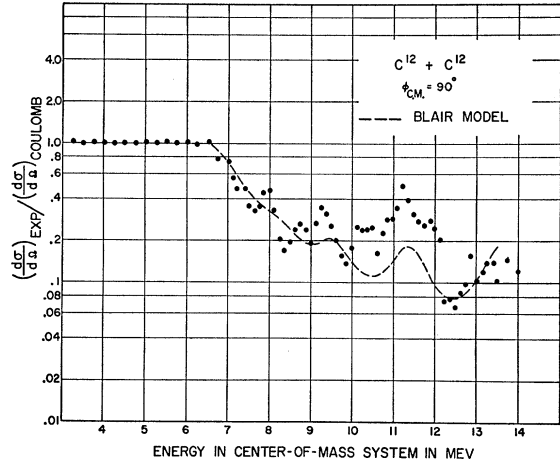


FIG. 21. Comparison of a Blair model calculation of the 90° $C^{12} + C^{12}$ elastic excitation curve with the experimental data.

been introduced into Eq. (12), giving

$$d\sigma/d\Omega = (Z^4 e^4 / 16E^2) \left| \csc^2(\phi/2) \exp[-i\eta \ln \sin^2(\phi/2)] + \sec^2(\phi/2) \exp[-i\eta \ln \cos^2(\phi/2)] + \frac{2}{i\eta} \sum_{l_{\text{even}}} (1 - A_l)(2l+1) \times \exp(2i\delta_l) P_l(\cos\phi) \right|^2, \quad (15)$$

where

$$\begin{aligned} A_l &= \frac{1}{2} - \frac{1}{2}(l' - l) \quad \text{for } |l' - l| \leq 1, \\ A_l &= 0 \quad \text{for } l < l' - 1, \\ A_l &= 1 \quad \text{for } l > l' + 1, \end{aligned} \quad (16)$$

and l' equals l_{\max} as given by Eq. (11). A feature of this particular definition is that the radius obtained using it corresponds to the radius obtained using an unmodified sharp-cutoff model at an energy where $l = l_{\max} + 1$. Thus a radius of 7.7 fermis obtained for $C^{12} + C^{12}$ using the sharp-cutoff model corresponds to a radius of 8.0 fermis using this modified model. The curve in Fig. 21 was obtained using the above modified sharp-cutoff model with $R = 8.0$ fermis. The calculated excitation function exhibits diffraction oscillations with an effective wavelength corresponding to ~ 2 Mev in the center-of-mass system. Diffraction structure of this wavelength has been observed in the $O^{16} + C^{12}$ system.³¹ While it is clear from Fig. 21 that underlying diffraction structure may well be present in the $C^{12} + C^{12}$ excitation function, there are superposed sharper and more irregular fluctuations. These fluctuations thus appear to correspond to narrow resonances in the compound system formed which have relatively large branching

³¹ J. A. Kuehner, E. Almqvist, and D. A. Bromley, Bull. Am. Phys. Soc. 5, 293 (1960), and to be published.

ratios for elastic decay. The corresponding resonant elastic amplitudes interfere with the Coulomb amplitudes to give the observed structure. These resonances are believed to be analogous to similar resonances having large Γ_c/Γ branching ratios observed in studies of the reaction products from C^{12} bombardment of C^{12} .⁷

It is worth noting that at the highest energies studied, the steep drop with increasing energy of the elastic scattering cross section at 90° for the $O+O$ system appears to terminate. Similar effects have been observed in other systems but in all cases extension of the data to higher energies will be required to see whether this effect is caused by onset of diffraction scattering as η becomes smaller or reflects some other phenomenon. It may be that nuclear elastic scattering at these energies corresponds to ~ 10 mb/sr and that the somewhat higher value for $C+C$ reflects an additional contribution from quasi-molecular states.

E. Resonance Analysis

As noted previously, the sharp structure corresponds to compound states with lifetime $\tau \sim 10^{-21}$ sec; the lack of correlation between structural features of the excitation curves at various angles of observation implies interference. From the magnitude of the fluctuations in the excitation curves it is possible to set approximate limits on the partial widths for remission of C^{12} nuclei, i.e., on the compound elastic widths. These approximate limits follow from the assumption that application of a single resonance formalism is valid. It is clear from the structure in the curves of Fig. 5 that overlapping levels are involved; however, rapid changes of yield over small energy intervals as in the region of $E=12.2$ Mev, for example, suggest the presence of a particular strong resonance.

The single-level formalism may be written as

$$\begin{aligned} d\sigma/d\Omega = & \left(Z^4 e^4 / 16E^2 \right) \left| \csc^2(\phi/2) \exp\{-i\eta \ln \sin^2(\phi/2)\} \right. \\ & + \sec^2(\phi/2) \exp\{-i\eta \ln \cos^2(\phi/2)\} \\ & - \frac{2i}{\eta} \sum_l (2l+1) P_l(\cos\phi) \\ & \times \exp(2i\delta_l) [1 - \exp(2iu_l)] \\ & - \frac{2i}{\eta} (2l'+1) P_{l'}(\cos\phi) \exp(2i\delta_{l'}) \\ & \left. \times \exp(2iu_{l'}) \frac{i\Gamma_c}{(E-E_0) + \frac{1}{2}i\Gamma} \right|^2, \quad (17) \end{aligned}$$

where in addition to the previously defined parameters u_l is the nuclear phase shift. The first term here is clearly the Coulomb amplitude, the last the specifically resonant amplitude, and the second the sum over non-resonant nuclear amplitudes. For convenience, param-

TABLE II. Calculated branching ratios for compound elastic decay.

l'	2	4	6	8	10	12	14	16
Γ_c/Γ	0.26	0.20	0.16	0.14	0.13	0.12	0.11	0.10

eters A and B_l may be defined by rewriting Eq. (17) as

$$\begin{aligned} \frac{d\sigma}{d\Omega} = & \frac{Z^4 e^4}{16E^2} \left| A + \sum_l B_l [1 - \exp(2iu_l)] \right. \\ & \left. + B_{l'} \exp(2iu_{l'}) \frac{i\Gamma_c}{\Delta E + \frac{1}{2}i\Gamma} \right|^2. \quad (18) \end{aligned}$$

In Fig. 5 resonant fluctuations of at least a factor of two are observed where $d\sigma/d\Omega$ at $\phi_{c.m.} = 90^\circ$ is $\sim \frac{1}{5}$ of the Coulomb prediction, i.e.,

$$\left(\frac{d\sigma}{d\Omega} \right) / \left(\frac{d\sigma}{d\Omega_{Coul}} \right) = \frac{|A + \sum_l B_l [1 - \exp(2iu_l)]|^2}{|A|^2} \approx \frac{1}{5};$$

since at $\phi_{c.m.} = 90^\circ$, $|A|^2 = 16$,

$$|A + \sum_l B_l [1 - \exp(2iu_l)]| \sim 4 \left(\frac{1}{5} \right)^{\frac{1}{2}}. \quad (19)$$

In order to produce average amplitude fluctuations of $\sim \sqrt{2}$ from Eqs. (18) and (19)

$$(|B_{l'} \Gamma_c| / \Gamma) \sim [(\sqrt{2}-1)/(\sqrt{2}+1)] \times 4 \times \left(\frac{1}{5} \right)^{\frac{1}{2}}, \quad (20)$$

whence

$$\Gamma_c/\Gamma \sim 0.307 / |B_{l'}|. \quad (21)$$

In the energy range from 8–14 Mev, $3.7 \leq \eta \leq 4.9$ and a value of 4.3 has been assumed for estimating purposes:

$$\frac{\Gamma_c}{\Gamma} \approx \frac{0.307\eta}{2(2l'+1) |P_{l'}(\cos\phi)|} = \frac{0.66}{(2l'+1) |P_{l'}(\cos\phi)|}. \quad (22)$$

Table II lists values of Γ_c/Γ as deduced from Eq. (22) as functions of the resonant orbital angular momentum ($l'=J$, the total angular momentum of the resonance, in this case of zero channel spin). As is clear from Table II, the fluctuations in the excitation curve of Fig. 5 imply surprisingly large values for the compound elastic branching ratio ranging from ~ 0.25 at low angular momenta to a relatively constant value of ~ 0.10 at high angular momenta.

It should be emphasized again that these estimates are based on the assumption of a single, isolated, resonant state. Since the physical situation involves overlapping states, this assumption leads to an uncertainty in the estimated branching ratio; on the average it would be expected that the presence of overlapping levels would result in an underestimate of Γ_c/Γ .

To summarize, then, the elastic scattering measurements reported here suggest that at energies above the Coulomb barrier in the $C+C$ system we are dealing with states which have lifetimes in excess of 10^{-21} sec,

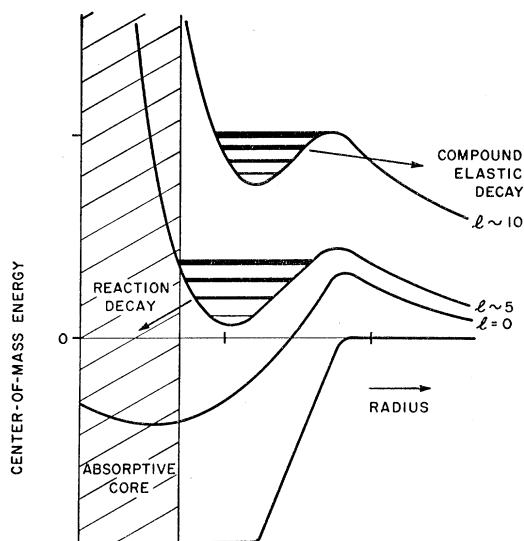


FIG. 22. Schematic interaction potential for the C+C system; resultant potential curves are shown for three representative orbital angular momenta.

which have a high branching ratio for compound elastic decay, and which appear to correspond to the resonant absorption of high partial waves. In contrast, no such states appear to contribute to the O+O scattering cross sections.

F. Quasi Molecules

The characteristics of the resonant states, i.e., large Γ_c/Γ and small Γ , as noted above have led in analogy to the metastable diatomic chemical molecule³² to the postulation of a quasi-molecular interaction mechanism,^{6,7,15,16} with the states in question being those in a secondary potential minimum at relatively large radius. Figure 22 shows a very schematic interaction potential for the C+C system of the type envisaged. The absorptive core implies that if two carbon nuclei attain separation radii in this range, they coalesce and thus lead eventually to reaction products.

Vogt and McManus¹⁵ have suggested that the outer maximum results from deformation of the carbon nuclei, while bound together following a grazing collision effectively by nuclear interactions in the overlap region at the collision interface. This suggestion is critically dependent upon the exact nuclear-structure characteristics of the nuclei involved and is an attractive one because it leads directly to differentiation between the C+C and O+O systems. In the former, overlap is readily permissible because of the 4 holes in the carbon p shell and because carbon is known to be relatively deformable; in the latter, the p shell is filled, inhibiting overlap, and the doubly-magic structure is unusually rigid, essentially eliminating the possibility of obtaining

a deformation potential maximum to bind the molecular states.

Davis, on the other hand, has suggested that the outer potential maximum is simply the reflection of the ordinary optical model potential appropriate to the system when added to the Coulomb and centrifugal potentials. At first sight these suggestions appear to be quite different; in particular the equilibrium "molecular" separation as proposed by Vogt and McManus¹⁵ is in the range from 7–10 f, whereas as proposed by Davis¹⁶ it is ~ 5 f. At first sight the former suggestion depends critically upon the nature of the ions involved, while the latter does not.

It must be borne in mind, however, that the optical model potential appearing in the Davis model¹⁶ must be that for the entire interacting system, and that the nuclear-structure differences already referred to between the C+C and O+O systems should be reflected in considerably different optical potentials. In particular, the greater deformability of the carbon nuclei would correspond to an optical model with a real part having a much longer shallow tail toward large interaction radii. With such a long tail, the models coalesce. It would clearly be of very considerable interest to attempt an optical model fit to the $d\sigma/d\Omega$ and $d\sigma/dE$ results at given E and Ω , respectively, presented herein; as yet only a preliminary attempt has been made to fit the $d\sigma/dE$ ³³ at $\phi_{c.m.} = 90^\circ$. However, further calculations of this sort are planned.

It should be borne in mind that there is yet another difference between the C+C and O+O systems as suggested previously,⁶ namely that nucleon transfer in the former case is entirely within the p shell, whereas in the latter the nucleons must transfer between the p and d shells. This change in orbital configuration would be expected to inhibit strongly the probability of such transfer and thus perhaps the probability of molecular binding.

With a quasi-molecular hypothesis of the sort advanced, the appearance of the strong resonant effects at energies above the barrier follows from the observation that with increasing energy, hence relative orbital angular momentum, the binding potential is distorted asymmetrically by the corresponding increase in the r^{-2} centrifugal potential to inhibit coalescence of the nuclei and favor a "compound" elastic decay. This is shown schematically in Fig. 21. On the other hand, with decreasing energy hence angular momentum, it would be expected that the binding potential would be distorted in the opposite sense to favor coalescence leading to reaction products from the Mg²⁴ compound system. These arguments suggested detailed examination of the low-energy reaction cross sections; as has been reported previously, in preliminary fashion, narrow resonances with large Γ_c/Γ have been observed under these

³² A. Avogadro, *J. Phys.* **73**, 58 (1811).

³³ H. Reeves, *Proceedings of the International Conference on Nuclear Structure*, edited by D. A. Bromley and E. W. Vogt (University of Toronto Press, Toronto, 1960), p. 964.

conditions in C+C but not in O+O, supporting the postulated reaction mechanism. A full report on these measurements, including further information and discussion bearing on the reaction mechanism, will be submitted for publication in the near future.

CONCLUSIONS

At energies below the Coulomb barriers, elastic scattering measurements on the C+C and O+O systems are in accord with the Mott-scattering predictions for identical spin-zero bosons. At higher energies evidence has been obtained for the existence of a quasi-molecular interaction mechanism present in the C+C but absent in the O+O system. It is suggested that this mechanism depends critically upon the characteristics of the component nuclei involved. Further measurements on the corresponding system reaction cross sections are suggested to provide further insight into the mechanism involved.

It is believed that this is the first evidence for such

molecular states in nuclear interactions; these states may provide an interesting probe for study of high-spin nuclear states as well as quasi-fission situations of particularly simple configuration. Further study of the binding involved in these states should provide significant information on the nature of the nuclear surfaces involved and on the nucleon interactions in the surfaces which give rise to the bond.

ACKNOWLEDGMENTS

We are indebted to a great many of our colleagues, in many laboratories, for discussions concerning these results; particular thanks are due Dr. E. W. Vogt and Dr. H. McManus. We would also express our appreciation to Dr. J. M. McKenzie for supplying the Au-Si detectors used and to Mr. W. Woytowich for preparing the carbon and silicon monoxide targets. We are indebted to C. E. L. Gingell for his assistance in instrumentation and to P. Ashbaugh and his associates for operation of the tandem accelerator.

Short-Lived Isomers of Ge⁷¹, As⁷⁴, Br⁷⁸, and Tc[†]

A. W. SCHARDT* AND ALBERT GOODMAN†

Los Alamos Scientific Laboratory, University of California, Los Alamos, New Mexico

(Received March 20, 1961)

Short-lived isomers have been produced with the pulsed beam of a Van de Graaff generator and observed between pulses with scintillation detectors. The results are summarized in the following table:

Isotope	Half-life	Isomeric transition (kev)	Observed gamma ray (kev)
Ge ⁷¹	20.3±0.3 msec	23 (<i>M2</i>)	175
As ⁷⁴	8.0±0.3 sec	283 (<i>M3</i>)	283±5
Br ⁷⁸	118.0±1.5 μsec	149 (<i>M2</i>)	149±2, 32±2
Tc	8.15±0.20 μsec		177±4
Tc	15.5±0.8 μsec		43±3

INTRODUCTION

ONE of the notable successes of the nuclear shell model has been the prediction of the islands of isomerism for odd nuclei.¹ The simple application of the predicted sequence of nucleon shells has led to the prediction of isomeric transitions characterized by a spin change of 3 or 4. In some cases the expected spin changes have not been found because of level shifts.

† Work performed under the auspices of the U. S. Atomic Energy Commission.

* Present address: Advanced Research Projects Agency, Washington 25, D. C.

† Present address: Sandia Corporation, Albuquerque, New Mexico.

¹ M. Goldhaber and R. D. Hill, *Revs. Modern Phys.* **24**, 179 (1952); M. Goldhaber and A. W. Sunyar, *Beta- and Gamma-Ray Spectroscopy*, edited by K. Siegbahn (Interscience Publishers, Inc., New York, 1955). Chap. 16, p. 453.

The disappearance of a $\Delta I = 3$ or 4 isomer may give rise instead to an *M2* isomer. For the region of 28 to 50 equivalent nucleons, the shell model predicts single-particle levels $p_{3/2}$, $f_{5/2}$, $p_{1/2}$, $g_{9/2}$, and also $7/2+$ and $5/2+$ levels formed by coupling of several equivalent $g_{9/2}$ nucleons. The island of isomerism is comprised of *M4* transitions between $g_{9/2}$ and $p_{1/2}$ levels and low-energy *E3* transitions between $7/2+$ and $p_{1/2}$ levels. However, *M2* isomers have been found² and the level configurations were $g_{9/2}-f_{5/2}$ (references 3 and 4) or

² *Nuclear Level Schemes, A=40-A=92*, compiled by K. Way, R. W. King, C. L. McGinnis, and R. van Lieshout, Atomic Energy Commission Report TID-5300 (U. S. Government Printing Office, Washington, D. C., 1955), and *Nuclear Data Sheets*, edited by C. L. McGinnis, National Academy of Sciences, National Research Council (U. S. Government Printing Office, Washington 25, D. C.).